IEEE Access
Multidisciplinary | Rapid Review | Open Access Journal

Received 28 July 2023, accepted 23 August 2023, date of publication 28 August 2023, date of current version 5 September 2023.

Digital Object Identifier 10.1109/ACCESS.2023.3309421

RESEARCH ARTICLE

Design and Analysis of Interior Permanent Magnet Motor With Magnetic Isolation and Heat Dissipation Integrated Auxiliary Slot

JINGFENG MAO[1], JIN HUANG[1], XINYU XU[1], JUNQIANG ZHENG[1], (Member, IEEE), AND XINXING ZHANG[2]

[1]School of Electrical Engineering, Nantong University, Nantong 226019, China
[2]Jingjiang College, Jiangsu University, Zhenjiang 212028, China

Corresponding author: Junqiang Zheng (zjq@ntu.edu.cn)

This work was supported in part by the Natural Science Research Program of Jiangsu Colleges and Universities under Grant 20KJA470002, Grant 23KJB470033, and Grant 21KJB470018; in part by the Postgraduate Research and Practice Innovation Program of Jiangsu Province under Grant SJCX22_1618; and in part by the National Natural Science Foundation of China under Grant 52307061.

ABSTRACT This paper presents a novel auxiliary slot interior permanent-magnet (IPM) motor. It not only plays the role of magnetic isolation and reduces the eddy-current (EC) loss, but also facilitates the ventilation and heat dissipation of the rotor. Initially, using a high-speed 6-slot and 4-pole IPM motor as an example, the structure characteristics of the auxiliary slot permanent-magnet (PM) motor with magnetic isolation and heat dissipation are explained. Subsequently, the finite-element method (FEM) is employed to conduct a multi-objective optimization design on the characteristic parameters of the auxiliary slot. Additionally, the electromagnetic performance of the 6-slot and 4-pole IPM motor is systematically analyzed and evaluated. Furthermore, the auxiliary slot structure was investigated to improve the efficiency of heat dissipation. The heat dissipation capacity of the auxiliary slot was further enhanced by analyzing various shapes of auxiliary slots. The results demonstrate that the proposed auxiliary slot structure can significantly reduce the EC loss and greatly improve the heat dissipation effect. Finally, the prototype is proofed by decreasing the volume, and the relevant experimental verification is carried out.

INDEX TERMS ANSYS Maxwell simulation, permanent-magnet motor, eddy-current loss, rotor auxiliary slot.

I. INTRODUCTION

Fractional-slot concentrated-winding (FSCW) PM motor has the advantages of a short winding end, high slot fulling, sinusoidal back-electromotive force (EMF) waveform, small torque ripple, and excellent fault-tolerant performance. It has significant applications in aerospace, military equipment, electric vehicles, ship propulsion, and other fields [1], [2], [3], [4]. However, the FSCW-PM motor has abundant magnet-motive force (MMF) harmonics, which will induce significant EC loss in the rotor PMs [5], [6], [7]. The rotor of the IPM motor makes it difficult to dissipate heat, and these heat accumulations exacerbate the motor temperature. It affects the output torque and causes irreversible PM demagnetization [8], [9], [10].

The suppression of EC loss is mainly by limiting the EC path, reducing stator MMF harmonics, and weakening the armature reaction magnetic field. Segment technology is the most commonly used method to reduce rotor EC loss. Its essence is to limit the EC path. In [11], [12], [13], [14], and [15], the axial and circumferential segmentation of PMs is carried out to increase the internal resistance of the EC loop, thereby reducing the EC loss. However, the segmentation will significantly increase the machining accuracy and difficulty of the brittle PM. In [16], [17], [18], [19], and [20], an EC loss suppression method with flux barriers on the rotor is systematically studied. The research shows that the rotor EC loss and core loss can be reduced due to the suppression of

The associate editor coordinating the review of this manuscript and approving it for publication was Qinfen Lu.

the low-order and long magnetic circuit armature reaction magnetic field harmonic by the flux barriers. However, this method isolates the rotor core, and the integrity of the rotor structure is threatened. Especially for the IPM motor, the application of this method will be limited.

Therefore, how to reduce the EC loss of the rotor and strengthen the heat dissipation effect of the high-speed rotor without affecting the main magnetic field and the mechanical properties is of great significance for the efficiency raising, energy saving, and quality improvement of electric equipment.

This paper proposes an auxiliary slot PM motor that integrates magnetic isolation and heat dissipation. It not only significantly reduces the EC loss, but also improves the effect of ventilation and heat dissipation without affecting the output torque performance. The arrangement of the article is as follows. Section II focuses on the structural characteristics of the auxiliary slot IPM motor. The multi-objective optimization of the characteristic parameters of the rotor auxiliary slots by the FEM is presented in Section III. Section IV systematically analyzes the electromagnetic performance of the optimized motor. With strengthening heat dissipation as the key goal, the topology of the auxiliary slot is explored and presented in Section V. Finally, the prototype is manufactured and verified by experiments.

II. STRUCTURAL CHARACTERISTICS OF AUXILIARY SLOT IPM MOTOR

A. MAGNETIC ISOLATION

Fig. 1 shows the distribution magnetic field of the IPM motor, including the PM magnetic field and armature reaction magnetic field. It should be noted that the left in Fig.1 (a) and (b) is the original IPM structure, and the right is the proposed IPM structure with the auxiliary slot. The rotor auxiliary slot is added between two adjacent PM poles. There are two essential principles for the design of the auxiliary slot: 1) Try not to affect the PM field; 2) Minimize the armature reaction magnetic field as much as possible to reduce the eddy current loss of the rotor [21], [22].

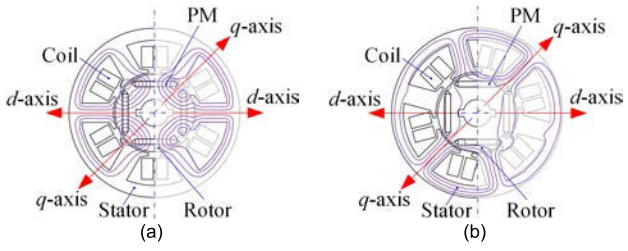

FIGURE 1. The distribution of magnetic field. (a) PM magnetic field. (b) Armature reaction magnetic field.

B. HEAT DISSIPATION CHANNELS

Except for the electromagnetic superiority, the designed auxiliary slot can also act as the heat dissipation vent of the high-speed rotor. It can accelerate the air convection heat transfer in the air gap, thereby enhancing the heat dissipation of the rotor. Fig. 2 exhibits the entire model of the motor and the schematic of the internal heat dissipation channel. The end of the housing adopts a hollow flange plate structure to strengthen the ventilation and heat dissipation of the motor. Combined with the auxiliary slot structure involved in this paper, the ventilation and heat dissipation effect of the small-volume high-speed motors can be further enhanced [23], [24].

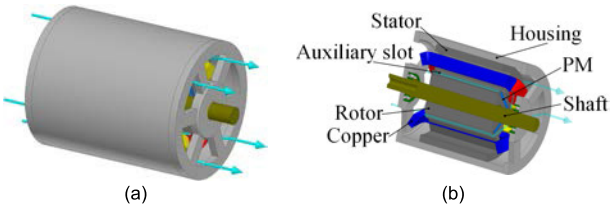

FIGURE 2. 3D motor model. (a) Entire model. (b) Heat dissipation channel.

III. OPTIMIZATION OF ROTOR AUXILIARY SLOT

The schematic of the auxiliary slot structure is presented in Fig. 3. The auxiliary slot width w_s and depth h_s are selected as the optimization variables in this paper, as shown in Fig. 3. During the optimization process, the slot width is quantitatively limited due to the distance limitation between two adjacent PM poles. The FEM is used to optimize the two variables of slot width and slot depth.

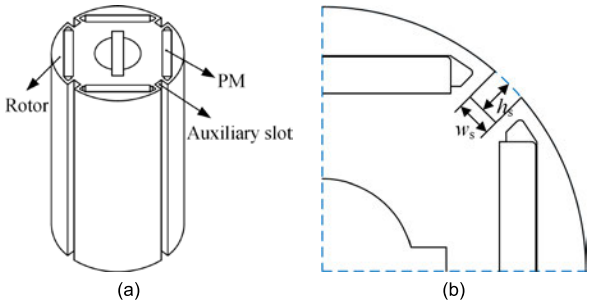

FIGURE 3. Auxiliary slot structure. (a) 3D schematic. (b) Auxiliary slot dimensioning diagram.

Fig. 4 presents the relationship between the amplitude of the no-load back-EMFs fundamental wave and the depth and width of the slot, and the relationship between the amplitude and the slot depth on the slot width of 3mm is superimposed (Limited by the distance between adjacent PMs). Overall, the larger the depth and width, the larger the amplitude of the fundamental wave, which shows that the auxiliary slot can suppress the magnetic flux leakage between the poles of the IPM motor, and the larger the slot, the more pronounced the suppression effect. Through the local analysis of the relationship between the fundamental amplitude and h_s, it can be seen that the amplitude first increases and then decreases with the slot depth, and the amplitude is constant in the range of 4-8mm. Fig. 5 shows the variation relationship of torque

with slot depth and width. Its variation trend is the same as in Fig. 4.

Fig. 6 exhibits the relationship between EC loss and the depth and width of the slot. The more significant the width and depth, the more obvious the suppression of the armature reaction magnetic field and the smaller the EC loss. However, when the width is 3mm, the EC loss decreases with the increase of the slot depth and tends to be gentle at a depth of 4mm.

Fig. 7 shows the relationship between the efficiency and the slot's depth and width. Due to the influence of the auxiliary slot on the torque and loss, the efficiency will change. Similarly, the larger the auxiliary slot, the more conducive to improving motor efficiency. When the width is fixed, the efficiency tends to be stable from the depth of 4mm.

In summary, under the condition that the width of the auxiliary slot is limited by space, the optimal depth point is 4mm, and the electromagnetic performance of all aspects is better at this time.

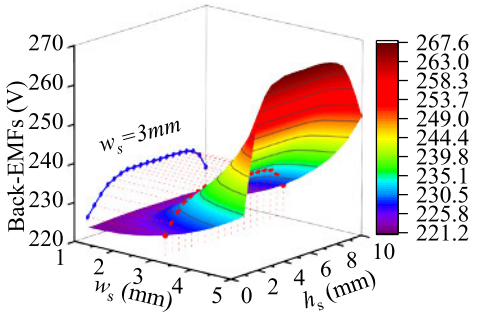

FIGURE 4. The relationship between the amplitude of the back-EMFs fundamental wave and the depth and width of the slot.

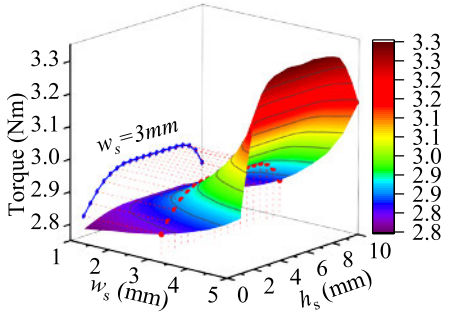

FIGURE 5. The relationship between torque and the depth and width of the slot.

IV. ELECTROMAGNETIC PERFORMANCE ANALYSIS

According to the optimization design results of electromagnetic performance, and considering the two factors of mechanical properties and heat dissipation capacity, the auxiliary slot depth of 4mm and the slot width of 3mm are selected for further electromagnetic performance analysis. The main design parameters of the two motors are shown in Table 1.

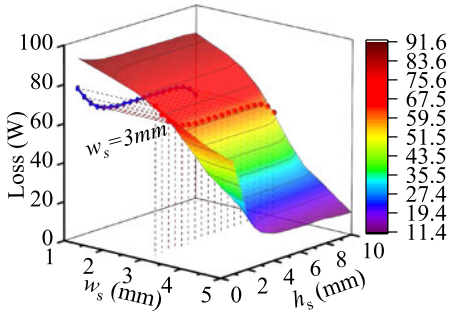

FIGURE 6. The relationship between EC loss and the depth and width of the slot.

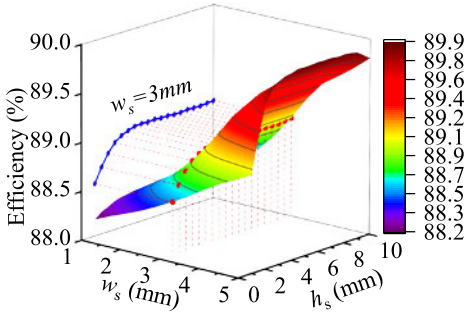

FIGURE 7. The relationship between efficiency and the depth and width of the slot.

TABLE 1. The main design parameters of the two motors.

	Original	Proposed
Stator outer diameter (mm)	90	90
Stator inside diameter (mm)	43.2	43.2
Axial length (mm)	75	75
Stator tooth width (mm)	10.3	10.3
Stator thickness (mm)	6.3	6.3
Air gap (mm)	0.9	0.9
Rotor outer diameter (mm)	41.4	41.4
Rotor inside diameter (mm)	14.4	14.4
Permanent magnet length (mm)	20.2	20.2
Permanent magnet thickness (mm)	2.9	2.9
Auxiliary slot width (mm)	/	3
Auxiliary slot depth (mm)	/	4

A. AIR GAP FLUX DENSITY ANALYSIS

Fig. 8 compares the air gap flux density under no-load conditions before and after slotting. Due to the magnetic isolation effect of the auxiliary slot, the magnetic flux leakage between the poles of the PM is effectively reduced, the peak value of the air gap flux density is improved, and the waveform is also changed. Its harmonic order shows that the suppression of magnetic flux leakage increases the flux density of the 2nd PM field harmonics, which improves motor torque.

Fig. 9 shows the armature reaction flux density of the motor. Compared with the original motor, the proposed auxiliary slot motor has some changes in the flux density waveform, and it can be found from its harmonic order that the 2nd harmonic of the armature reaction flux density is reduced by about 10%. Although this harmonic is a working harmonic,

the increase of the PM flux density harmonic will not reduce output torque. In addition, the reduction of armature reaction field harmonics will reduce the harmonic losses of the motor.

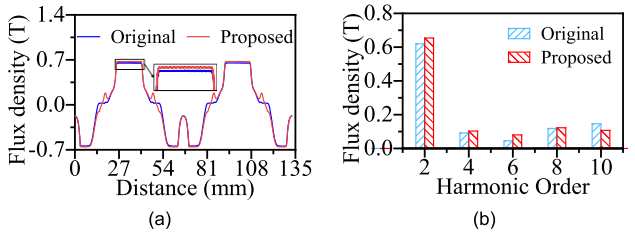

FIGURE 8. No-load flux density waveform and harmonic order. (a) Waveform. (b) Harmonic order.

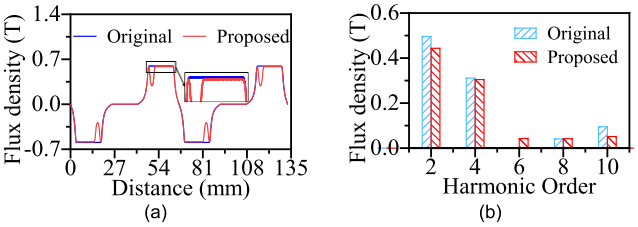

FIGURE 9. Armature response flux density waveform and harmonic order. (a) Waveform. (b) Harmonic order.

B. NO-LOAD BACK-EMFS

Fig. 10 compares the no-load magnetic lines of the PM motor with and without auxiliary slots. The auxiliary slot of the rotor slightly adjusts the magnetic circuit of the PM field. However, it hardly affects the flux density of the PM, which is also the essential principle of the design of the auxiliary slot.

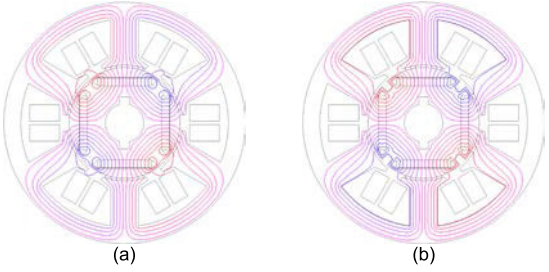

FIGURE 10. No-load magnetic lines. (a) Original. (b) Proposed.

Fig. 11 contrasts the no-load back-EMFs waveform and harmonic order of the two PM motors. Generally, the auxiliary slot has little effect on the no-load back-EMFs waveform of the motor. The waveform is relatively sinusoidal, the peak is in a spike state, and the amplitude is about 250V. This is because it contains a sizeable 5th harmonic, which can also be seen in its harmonic order. In addition, the auxiliary slot can increase the back-EMFs of the motor, and the fundamental amplitude is increased from 222.4V to 234.1V, which is increased by about 5%.

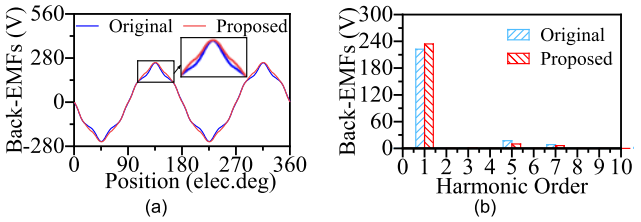

FIGURE 11. No-load back-EMFs waveform and harmonic order. (a) Waveform. (b) Harmonic order.

C. TORQUE

The saturation degree of the magnetic circuit is an essential determinant factor affecting the output capacity of the motor. The load flux density figure can intuitively characterize the saturation degree of the motor magnetic circuit. In the flux density range of 0 ∼ 2T, the load flux density distribution of the two structures is depicted in Fig. 12. It can be found that due to the existence of the auxiliary slot, the saturation degree of the motor is improved to a certain extent, which helps to obtain greater torque output.

Fig. 13 shows the output torque of two different schemes. After slotting, the average output torque is increased from 2.7Nm to 2.9Nm, about 7.4% higher than the original. The torque ripple is also reduced from 32% to 21.1%.

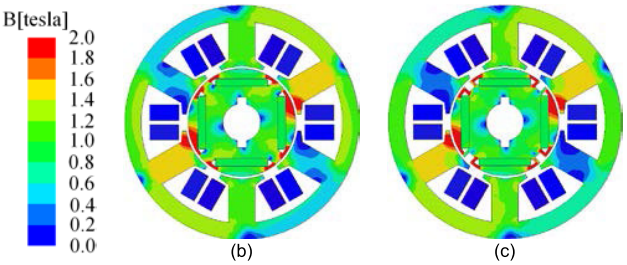

FIGURE 12. Load flux density. (a) Original. (b) Proposed.

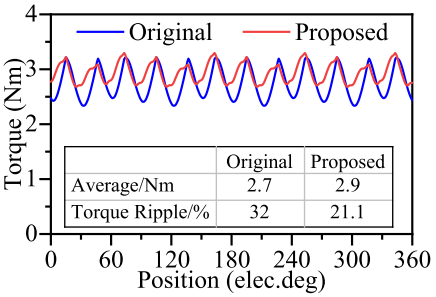

FIGURE 13. Output torque.

D. ELECTROMAGNETIC LOSS

Fig. 14 presents the iron loss of the two motors at the rated load. The iron loss is slightly reduced after slotting, from 222.3W to 211W, which is reduced by about 5%.

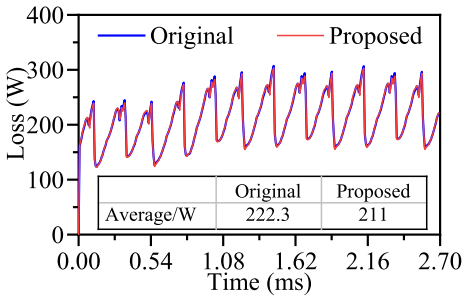

FIGURE 14. Total iron loss.

Fig. 15 compares the EC loss of the PM before and after slotting. It can be seen that the EC loss after the rotor slotting is significantly reduced, from 98.4W to 60.5W.

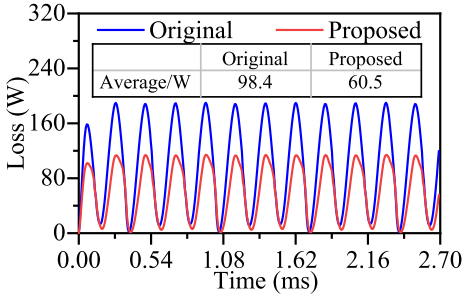

FIGURE 15. PM EC loss.

The temperature distribution of two different rotor structures is described in Fig. 16. The maximum temperature of the rotor after slotting is reduced from 113.6 °C to 92.8 °C. It can be seen that the auxiliary slot structure has a particular effect on heat dissipation.

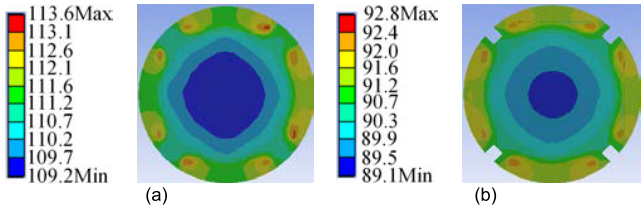

FIGURE 16. Rotor temperature distribution. (a) Original. (b) Proposed.

V. STRUCTURE EXPANSION OF ROTOR AUXILIARY SLOT

The original motor has a sizeable no-load current, mainly caused by the fan at the end of the motor. The fan plays an essential role in heat dissipation and ventilation. It is difficult to remove or replace it. In other words, reducing the no-load current and strengthening the heat dissipation is contradictory on the technology. The integrated design of the fan and high-speed PM rotor is critical to achieving low no-load current and ensuring high heat dissipation. Therefore, a new coupled rotor structure is proposed in this paper. The structure can not only improve the electromagnetic performance, but also act as a fan with a favorable heat dissipation function. As shown in Fig.17 (a), this paper improves the electromagnetic performance and strengthens the heat dissipation by adding a straight slot on the axial surface of the rotor. Fig. 17 (b) and Fig. 17 (c) are further extensions of this paper. Changing the shape of the slot increases the heat dissipation area, improves the working surface, and further improves the heat dissipation effect.

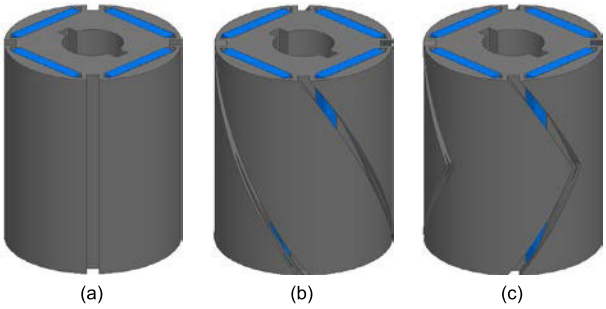

FIGURE 17. Rotor auxiliary slot structure. (a) Straight slot. (b) Skew slot. (c) V-shaped slot.

Fig. 18 is the wind speed distribution of the rotor auxiliary slot. It can be seen that after the skew slot is added, the axial ventilation capacity of the rotor is improved. Compared with the straight slot, it has a specific effect on heat dissipation, but the result is not apparent. In contrast, the V-shaped slot structure is more pronounced, which can accelerate the flow of air inside the motor and play a more significant role in heat dissipation.

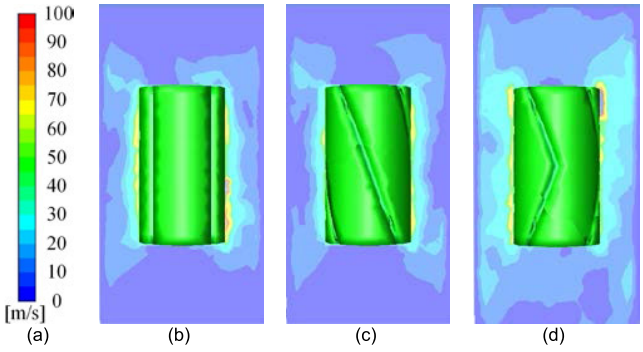

FIGURE 18. Wind speed distribution of rotor auxiliary slot. (a) Legend. (b) Straight slot. (c) Skew slot. (d) V-shaped slot.

VI. EXPERIMENTAL VERIFICATION

A. PROOFING OF PROTOTYPE

Based on previous analysis, this part verifies the motor by experiments. Considering the cost of the motor, the motor is reduced in equal proportion, and the prototype is exhibited in Fig. 19.

B. EVALUATION OF TEST RESULTS

Firstly, the performance of the motor with a fan was tested. Fig. 20 shows the efficiency test curves under different load

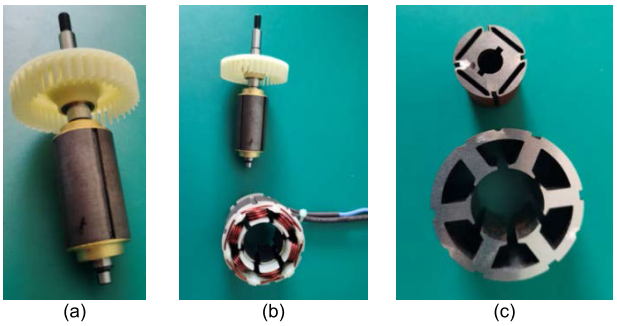

FIGURE 19. Prototype. (a) Rotor. (b) Rotor and winding. (c) Stator and rotor.

torques. The efficiency of the proposed motor is higher than that of the original motor in the whole load range. The efficiency improvement in the load torque range of 100 ∼ 200mNm is relatively significant. It is estimated that the efficiency of this interval is increased by about 2.3 ∼ 3.2%. According to the previous demonstration, the rated torque of this motor is about 200mNm, and the efficiency is increased by about 2.7% at this load point.

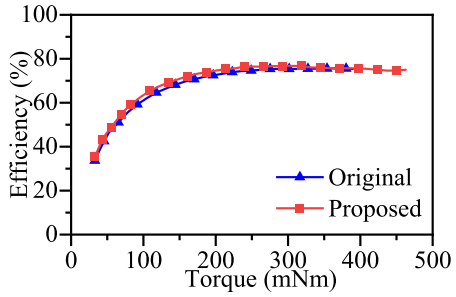

FIGURE 20. Efficiency test curves under different load torques.

Fig. 21 depicts the current test curves under different load torques. The current of the proposed motor is lower than the original motor in the whole load range. Under the same output torque, the smaller the current required, the stronger the overload capacity of the motor. According to the test data shown in Fig. 21, the proposed motor significantly improves the overload capacity, which is conducive to improving the performance of the entire product.

C. OPTIMIZED MOTOR FANLESS TEST

Immediately after this, the case without a fan was tested. Fig. 22 presents the efficiency test curves under different load torques. Obviously, the efficiency is greatly improved in the whole load range under the condition of no fan, especially in the load torque range of 100 ∼ 200mNm. After calculation, the efficiency in this range is increased by about 12 ∼ 19%. At the rated torque working point of the motor, the efficiency is increased by about 11.6%.

Fig. 23 illustrates the current test curves under different load torques. The proposed motor has enhanced overload

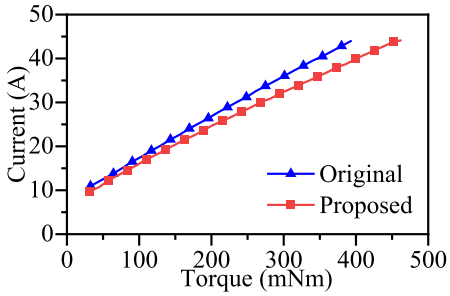

FIGURE 21. Current test curves under different load torques.

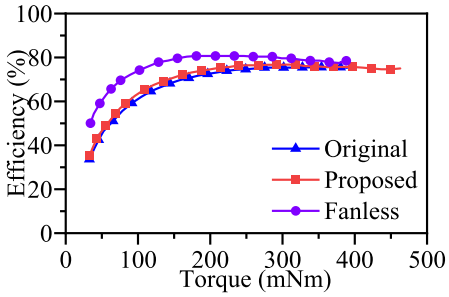

FIGURE 22. Efficiency test curves under different load torques.

performance (especially in the low torque region) without a fan, dramatically improving motor performance.

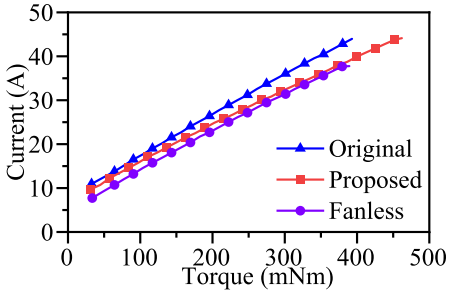

FIGURE 23. Current test curves under different load torques.

In summary, the proposed motor has a specific improvement in efficiency when there is a fan, increasing by about 2.3∼3.2%, and the overload performance is also enhanced. In the case of no fan, the efficiency has been more significantly improved by about 12 ∼ 19%, and the overload capacity has been further enhanced. Therefore, the proposed motor substantially improves the performance of the original, which is worthy of popularization and application.

VII. CONCLUSION

This paper proposes an IPM brushless motor with a rotor auxiliary slot. The interior one-type rotor structure is adopted, and an open slot is designed between the poles of two adjacent PMs. This structure can reduce the magnetic flux leakage between the poles of two adjacent PMs, improve the utilization rate of the PM, and reduce the EC loss to a certain

extent, which is beneficial to improving motor efficiency. In addition, the auxiliary slot acts as the heat dissipation channel of the rotor to enhance the convective heat transfer capacity of the air inside the motor, which is profitable for ventilation and heat dissipation. In addition to the above, the structure can reduce the torque ripple to a certain extent. The specific research results are as follows:

1) Reasonable rotor auxiliary slot design can improve the air gap flux density, increase the output torque, and suppress the torque ripple.

2) The rotor auxiliary slot design can reduce the harmonic content of the flux density waveform and reduce the eddy current loss.

3) A magnetic isolation slot is added to the rotor to form a structured design similar to a 'fan', which abandons the external fan. While reducing the load, the air in the air gap maintains a high convective heat transfer capacity. While improving the efficiency, the temperature of the rotor is effectively reduced.

REFERENCES

[1] W. Geng, Y. Wang, J. Wang, J. Hou, J. Guo, and Z. Zhang, "Comparative study of yokeless stator axial-flux PM machines having fractional slot concentrated and integral slot distributed windings for electric vehicle traction applications," *IEEE Trans. Ind. Electron.*, vol. 70, no. 1, pp. 155–166, Jan. 2023.

[2] C. Zhou, X. Huang, Z. Li, and W. Cao, "Design consideration of fractional slot concentrated winding interior permanent magnet synchronous motor for EV and HEV applications," *IEEE Access*, vol. 9, pp. 64116–64126, 2021.

[3] X. Fan, B. Zhang, R. Qu, D. Li, J. Li, and Y. Huo, "Comparative thermal analysis of IPMSMs with integral-slot distributed-winding (ISDW) and fractional-slot concentrated-winding (FSCW) for electric vehicle application," *IEEE Trans. Ind. Appl.*, vol. 55, no. 4, pp. 3577–3588, Jul. 2019.

[4] A. M. El-Refaie, "Fractional-slot concentrated-windings synchronous permanent magnet machines: Opportunities and challenges," *IEEE Trans. Ind. Electron.*, vol. 57, no. 1, pp. 107–121, Jan. 2010.

[5] L. Guo, J. Xu, S. Wu, X. Xie, and H. Wang, "Analysis and design of dual three-phase fractional-slot permanent magnet motor with low space harmonic," *IEEE Trans. Magn.*, vol. 58, no. 1, pp. 1–12, Jan. 2022.

[6] X. Chen and J. Wang, "Magnetomotive force harmonic reduction techniques for fractional-slot non-overlapping winding configurations in permanent-magnet synchronous machines," *Chin. J. Electr. Eng.*, vol. 3, no. 2, pp. 102–113, Sep. 2017.

[7] X. Teng, Y. Li, B. Zhang, G. Feng, and Z. Liu, "Rotor loss analysis of an external rotor high-speed permanent magnet motor considering current harmonics and thermal analysis under high-temperature gas," *IEEJ Trans. Electr. Electron. Eng.*, vol. 18, no. 4, pp. 623–638, Apr. 2023.

[8] J. Liu, Y. Liang, P. Yang, W. Wang, F. Zhao, and K. Xu, "Analysis on circulating current loss in the formed winding of permanent magnet synchronous motors," *IEEE Access*, vol. 9, pp. 113403–113414, 2021.

[9] M.-M. Koo, J.-Y. Choi, K. Hong, and K. Lee, "Comparative analysis of eddy-current loss in permanent magnet synchronous machine considering PM shape and skew effect using 3-D FEA," *IEEE Trans. Magn.*, vol. 51, no. 11, pp. 1–4, Nov. 2015.

[10] E. Fornasiero, N. Bianchi, and S. Bolognani, "Slot harmonic impact on rotor losses in fractional-slot permanent-magnet machines," *IEEE Trans. Ind. Electron.*, vol. 59, no. 6, pp. 2557–2564, Jun. 2012.

[11] T. Li, Y. Zhang, Y. Liang, Y. Yang, and J. Jiao, "Magnet eddy-current losses reduction of an axial-flux in-wheel motor with amorphous magnet metal," *Int. J. Appl. Electromagn. Mech.*, vol. 65, no. 3, pp. 431–450, Mar. 2021.

[12] Y. Hu, S. Zhu, and C. Liu, "Magnet eddy-current loss analysis of interior PM machines for electric vehicle application," *IEEE Trans. Magn.*, vol. 53, no. 11, pp. 1–4, Nov. 2017.

[13] P. Su, W. Hua, M. Hu, Z. Chen, M. Cheng, and W. Wang, "Analysis of PM eddy current loss in rotor-PM and stator-PM flux-switching machines by air-gap field modulation theory," *IEEE Trans. Ind. Electron.*, vol. 67, no. 3, pp. 1824–1835, Mar. 2020.

[14] B.-C. Kim, J.-H. Lee, and D.-W. Kang, "A study on the effect of eddy current loss and demagnetization characteristics of magnet division," *IEEE Trans. Appl. Supercond.*, vol. 30, no. 4, pp. 1–5, Jun. 2020.

[15] Y. Wang, J. Ma, C. Liu, G. Lei, Y. Guo, and J. Zhu, "Reduction of magnet eddy current loss in PMSM by using partial magnet segment method," *IEEE Trans. Magn.*, vol. 55, no. 7, pp. 1–5, Jul. 2019.

[16] G. Choi and T. M. Jahns, "Reduction of eddy-current losses in fractional-slot concentrated-winding synchronous PM machines," *IEEE Trans. Magn.*, vol. 52, no. 7, pp. 1–4, Jul. 2016.

[17] J. Luo, W. Zhao, J. Ji, J. Zheng, Y. Zhang, Z. Ling, and J. Mao, "Reduction of eddy-current loss in flux-switching permanent-magnet machines using rotor magnetic flux barriers," *IEEE Trans. Magn.*, vol. 53, no. 11, pp. 1–5, Nov. 2017.

[18] T. A. Huynh, J.-X. Peng, M.-F. Hsieh, and P.-W. Huang, "Anti-demagnetization analysis of fractional slot concentrated windings interior permanent magnet motor considering effect of rotor design parameters," *IEEE Trans. Magn.*, vol. 58, no. 2, pp. 1–6, Feb. 2022.

[19] E. Sayed, Y. Yang, B. Bilgin, M. H. Bakr, and A. Emadi, "A comprehensive review of flux barriers in interior permanent magnet synchronous machines," *IEEE Access*, vol. 7, pp. 149168–149181, 2019.

[20] J. Zheng, W. Zhao, J. Ji, J. Zhu, C. Gu, and S. Zhu, "Design to reduce rotor losses in fault-tolerant permanent-magnet machines," *IEEE Trans. Ind. Electron.*, vol. 65, no. 11, pp. 8476–8487, Nov. 2018.

[21] S. Wu, L. Guo, H. Wang, Z. Wang, Z. Song, and T. Shi, "Analytical calculation for magnetic field in spoke-type permanent magnet machines based on a rotor magnetic potential model," *IEEE Trans. Magn.*, vol. 58, no. 2, pp. 1–5, Feb. 2022.

[22] J. Zheng, W. Zhao, J. Ji, J. Zhu, and C. H. T. Lee, "Sleeve design of permanent-magnet machine for low rotor losses," *Chin. J. Electr. Eng.*, vol. 6, no. 4, pp. 86–96, Dec. 2020.

[23] J. Dong, Y. Huang, L. Jin, and H. Lin, "Comparative study of surface-mounted and interior permanent-magnet motors for high-speed applications," *IEEE Trans. Appl. Supercond.*, vol. 26, no. 4, pp. 1–4, Jun. 2016.

[24] J. K. Si, L. F. Zheng, and H. C. Feng, "Analysis of 3-D temperature field for surface-mounted and interior permanent magnet synchronous motor," *Electr. Mach. Control*, vol. 21, no. 3, pp. 25–31, 2017.

JINGFENG MAO received the B.Eng. degree in industrial automation from the School of Automation, Wuhan University of Technology, Wuhan, China, in 1998, and the M.Sc. and Ph.D. degrees in electric engineering from the School of Electrical and Information Engineering, Jiangsu University, Zhenjiang, China, in 2004 and 2008, respectively.

Since 1998, he has been with Nantong University, Nantong, China, where he is currently a Professor with the School of Electrical Engineering. His research interests include electrical machines and drives, renewable energy generations and applications, and control and design of microgrids.

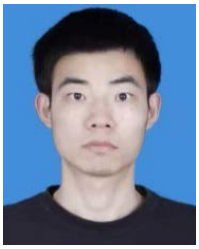

JIN HUANG received the B.Eng. degree in measuring and control technology and instrumentations from Nantong University, Nantong, China, in 2021.

His research interests include electric machine design and thermal analysis.

XINYU XU received the B.Eng. degree in electrical engineering and intelligent control from Nantong University, Nantong, China, in 2020, where he is currently pursuing the M.Sc. degree.

His research interests include interior permanent-magnet machine design and harmonic analysis.

JUNQIANG ZHENG (Member, IEEE) received the B.Sc. and Ph.D. degrees in electrical engineering from Jiangsu University, Zhenjiang, China, in 2014 and 2021, respectively.

From 2019 to 2020, he was a Visiting Student with the School of Electrical and Electronic Engineering, Nanyang Technological University, Singapore. He has been with Nantong University, Nantong, China, since 2021, where he is currently a Lecturer with the School of Electrical Engineering. His research interests include electric machine design, modeling, fault-tolerant, space harmonic, loss analysis, and electromagnetic field computation.

XINXING ZHANG received the B.S. and M.S. degrees from Jiangsu University, Zhenjiang, China.

She is currently with the Jingjiang College, Jiangsu University. Her research interests include computation of electromagnetic fields for permanent-magnet motor and motor design.